Structure
Article

Structural Basis for Ca^{2+}-Dependent Formation of ALG-2/Alix Peptide Complex: Ca^{2+}/EF3-Driven Arginine Switch Mechanism

Hironori Suzuki,[1,3] Masato Kawasaki,[2,3] Tatsutoshi Inuzuka,[1] Mayumi Okumura,[1] Takeshi Kakiuchi,[1] Hideki Shibata,[1] Soichi Wakatsuki,[2] and Masatoshi Maki[1,*]
[1]Department of Applied Molecular Biosciences, Graduate School of Bioagricultural Sciences, Nagoya University, Nagoya 464-8601, Japan
[2]Structural Biology Research Center, Photon Factory, Institute of Materials Structure Science, High Energy Accelerator Research Organization (KEK), Tsukuba, Ibaraki 305-0801, Japan
[3]These authors contributed equally to this work.
*Correspondence: mmaki@agr.nagoya-u.ac.jp
DOI 10.1016/j.str.2008.07.012

SUMMARY

ALG-2 belongs to the penta-EF-hand (PEF) protein family and interacts with various intracellular proteins, such as Alix and TSG101, that are involved in endosomal sorting and HIV budding. Through X-ray crystallography, we solved the structures of Ca^{2+}-free and -bound forms of N-terminally truncated human ALG-2 (des3-20ALG-2), Zn^{2+}-bound form of full-length ALG-2, and the structure of the complex between des3-23ALG-2 and the peptide corresponding to Alix799-814 in Zn^{2+}-bound form. Binding of Ca^{2+} to EF3 enables the side chain of Arg125, present in the loop connecting EF3 and EF4, to move enough to make a primary hydrophobic pocket accessible to the critical PPYP motif, which partially overlaps with the GPP motif for the binding of Cep55 (centrosome protein 55 kDa). Based on these results, together with the results of in vitro binding assay with mutant ALG-2 and Alix proteins, we propose a Ca^{2+}/EF3-driven arginine switch mechanism for ALG-2 binding to Alix.

INTRODUCTION

ALG-2 is an apoptosis-linked calcium-binding protein of 191 amino acid residues containing five serially repetitive EF-hand motifs (EF1–EF5) in its C-terminal region, and belongs to the penta-EF-hand (PEF) family, which includes the calpain small subunit, sorcin, grancalcin, and peflin in mammals (reviewed by Maki et al. [1997; 2002]). Among the mammalian PEF proteins, ALG-2 has the shortest Gly/Pro-rich hydrophobic region (23 residues) in its N-terminal region. ALG-2 was identified as a proapoptotic protein of a mouse T-cell hybridoma, and it was found that ALG-2 depletion by expression of its antisense mRNA protects against cell death induced by several stimuli, such as glucocorticoids, T-cell receptors, and Fas triggering (Vito et al., 1996). ALG-2 has been shown to interact Ca^{2+}-dependently with various intracellular proteins containing Pro-rich regions, such as Alix (also known as AIP1) (Missotten et al., 1999; Vito et al., 1999), annexins A7 and A11 (Satoh et al., 2002a, 2002b), TSG101 (Katoh et al., 2005), and phospholipid scramblase 3 (Shibata et al., 2008). Although ALG-2-deficient mice develop normally with no obvious abnormalities in the immune systems (Jang et al., 2002), it has been suggested that ALG-2 and/or Alix have physiological roles in regulation of ER-stress-induced apoptosis, neuronal cell death during development, and cancer (Rao et al., 2004; reviewed by Tarabykina et al. [2004]; Sadoul [2006]; Maki and Shibata [2007]). Alix functions in the regulation of cell adhesion, apoptosis, endocytosis, multivesicular body formation, and budding of enveloped RNA viruses (Morita and Sundquist, 2004; Odorizzi, 2006). Alix is a cytoplasmic 95 kDa protein containing Bro1 domain, V domain, and Pro-rich domain in the N-terminal, middle, and C-terminal regions, respectively (Williams and Urbé, 2007). ALG-2 binds Alix in the C-terminal Pro-rich region at a site that contains four tandem PxY repeats (Shibata et al., 2004). Simultaneous substitutions of all four prolines or tyrosines to alanines caused loss of the binding ability, but it has remained unclear which Pro or Tyr residues are critical for the interaction. An alternative splicing isoform lacking Gly121-Phe122, designated ALG-$2^{\Delta GF122}$ in this article, does not bind Alix (Tarabykina et al., 2000; Shibata et al., 2007, 2008).

X-ray crystal structures of PEF proteins have been solved for calpain subunits (Blanchard et al., 1997; Lin et al., 1997; Hosfield et al., 1999; Strobl et al., 2000) and their close homologs, such as sorcin (Xie et al., 2001; Ilari et al., 2002) and grancalcin (Jia et al., 2000, 2001a). Each PEF protein contains eight α helices and forms a dimer via EF5. Although the crystal structure of the Ca^{2+}-bound form of elastase-treated mouse ALG-2 has also been solved (Jia et al., 2001b), structures of the Ca^{2+}-free form and complexes with target peptides have remained unknown. In the present study, we elucidate the crystal structures of the Ca^{2+}-free form, the Ca^{2+}-bound form, the Zn^{2+}-bound form, and the Alix oligopeptide complex with either full-length or N-terminal Gly/Pro segment-deleted human ALG-2. Based on a comparison of these structures and the results of in vitro binding assays with mutant ALG-2 and Alix proteins, we postulate the structural basis for the mechanism of Ca^{2+}-dependent binding of ALG-2 to Alix at the atomic level. Binding of Ca^{2+} to EF3 induces rearrangement of the loop connecting EF3 and EF4, and makes a hydrophobic pocket accessible to the primary binding site of Alix peptide.

RESULTS AND DISCUSSION

For crystallization of human ALG-2, we prepared recombinant proteins in the forms of full-length and two different mutants with deletion in the N-terminal Gly/Pro-rich region (des3-20ALG-2; des3-23ALG-2) (Figure 1). Crystallization conditions were first screened with an automated robotic system (Hiraki et al., 2006) and further optimized manually. All crystal structures were solved by the molecular replacement method with the program MOLREP (Vagin and Teplyakov, 1997), with the Ca^{2+}-bound structure of elastase-treated mouse ALG-2 (Jia et al., 2001b) (Protein Data Bank [PDB] code 1HQV) as a search model. Data collection, processing, and refinement statistics are summarized in Table S1 available online. Schematic secondary structures and Ca^{2+}-coordinating residues are shown alongside the amino acid sequence in Figure S1.

Jia et al. (2001a; 2001b) previously compared the elucidated crystal structure of Ca^{2+}-bound mouse ALG-2 with the Ca^{2+}-free and -bound forms of grancalcin and calpain domain VI (dVI; small subunit PEF domain). However, structural comparison between Ca^{2+}-bound ALG-2 and either Ca^{2+}-free grancalcin or calpain dVI gave limited information, because ALG-2 belongs to the group I PEF subfamily and it is evolutionarily distant from members of the group II PEF subfamily that includes calpain subunits, grancalcin and sorcin (Maki et al., 2002). Vernarecci et al. (2007) recently found by fluorescence photometric analyses that the yeast homolog of ALG-2, Pef1p, binds both Ca^{2+} and Zn^{2+}, and that both ions induce conformational change of the protein. Indeed, zinc ion was also found to be effective for human ALG-2 to interact with Alix peptide with a surface plasmon resonance (SPR) biosensor (Figure S2).

Structures of Ca^{2+}-Free, Ca^{2+}-Bound, and Zn^{2+}-Bound ALG-2 Proteins

We investigated Ca^{2+}- or Zn^{2+}-induced conformational changes by solving the structures of Ca^{2+}-free and Ca^{2+}-bound forms of des3-20ALG-2 (PDB codes 2ZND and 2ZN9, respectively) and the Zn^{2+}-bound form of full-length ALG-2 (PDB code 2ZN8). In agreement with the mouse ALG-2 crystal structure, calcium ions were found in the loops of EF1, EF3, and EF5 of the human des3-20ALG-2 crystal, and were coordinated at x, y, z, −y, −x, and −z positions, as summarized in Table 1. Water molecule at the −x canonical coordination position is absent in the EF3 structure. Among the PEF proteins, ALG-2 is unique in that its EF5 binds Ca^{2+} in a canonical coordination, except for the −z position. A fourth calcium atom is held by two Asn106 residues in crystallographically symmetric ALG-2 molecules (data not shown). Coordination of zinc ions in EF1 and EF3 is similar to that of calcium ions, except that water molecule at the −x canonical coordination position is absent in the EF1 structure (Table 1). An electron density map shows that there are two ions bound in the EF5 loop region. Anomalous difference Fourier map at 1.0 Å wavelength X-ray, however, indicates that the ion coordinated at the canonical x, y, z, and −y positions is not Zn^{2+}. Instead of Zn^{2+}, another ion is coordinated at x, y, z, and −y positions. Since the crystallization buffer contains sodium salt, the coordinated ion at the canonical positions in EF5 may be Na^{+}. Coordination of Na^{+} was indeed recently reported for Ca^{2+}-free S100A2 crystal structure (Koch et al., 2008). On the other hand, the second ion that binds to $OD1^{D171}$ shows a strong anomalous signal of Zn^{2+} (data not shown).

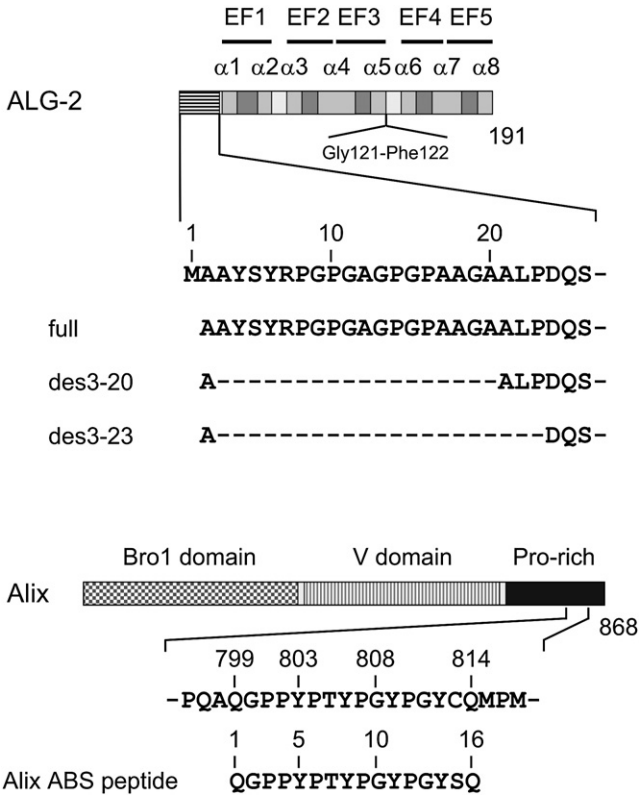

Figure 1. Schematic Representations of ALG-2 and Alix

Human ALG-2 has a Gly/Pro-rich N-terminal region followed by the PEF domain containing five EF-hands (EF1–EF5) with eight α helices (α1–α8). The first and second helices in each EF hand are alternatively named, for instance, helix E1 and helix F1, respectively. An alternatively spliced isoform (lacking Gly121-Phe122) is designated ALG-$2^{\Delta GF122}$ in this article. Recombinant proteins of full-length ALG-2 and two types of N-terminal deletion mutants (des3-20ALG-2 and des3-23ALG-2) were crystallized. Alix has three distinct domains, named Bro1, V, and Pro-rich. A 16-mer synthetic oligopeptide of the ABS in Alix (Alix ABS peptide) was used for cocrystallization.

Ca^{2+}- or Zn^{2+}-Induced Conformational Changes

The structures aligned between human des3-20ALG-2 and mouse des1-20ALG-2 have a root-mean-square deviation (rmsd) value of 0.21 Å for C^{α} atoms from residues Ala21 to Phe188, indicating extremely similar structures. On the other hand, the aligned structures between the Ca^{2+}-free and Ca^{2+}-bound form of human des3-20ALG-2 have an rmsd value of 1.20 Å for C^{α} atoms from residues Gln25 to Ser189 (Figure S3). The resolved overall structure of the Zn^{2+}-bound form of full-length ALG-2 is very similar to that of the Ca^{2+}-bound form of des3-20ALG-2, except for EF5s (rmsd, 0.76 Å for C^{α} atoms from residues 26–189) (Figure S3). The N-terminal Gly/Pro-rich region of full-length ALG-2 is not visible in the electron density map.

As shown in Figures 2A–2C, canonical 12 residue EF-hand Ca^{2+}-coordinating loops are formed between two almost perpendicularly placed helices in EF1 (α1 and α2) and EF3 (α4 and α5), whereas EF5 has two extra residue insertions in the loop

Table 1. Bond Distance for the Divalent Ion Coordinate in ALG-2

	EF1			EF3			EF5		
		Distance (Å)			Distance (Å)			Distance (Å)	
		Ca^{2+}	Zn^{2+}		Ca^{2+}	Zn^{2+}		Ca^{2+}	Zn^{2+}
Position	Atom	des3-20[a]	Full[b]	Atom	des3-20	Full	Atom	des3-20	Full
x	$OD1^{D36}$	2.3	2.2	$OD1^{D103}$	2.3	2.3	$OD1^{D169}$	2.5	ND
y	$OD2^{D38}$	2.2	2.3	$OD2^{D105}$	2.5	2.4	$OD2^{D171}$	2.3	ND
z	OG^{S40}	2.8	2.5	OG^{S107}	2.5	2.8	$OD1^{D173}$	2.2	ND
−y	O^{V42}	2.4	2.1	O^{M109}	2.4	2.5	O^{W175}	2.5	ND
−x	H_2O	2.3	ND	H_2O	ND	2.8	H_2O	2.3	ND
−z	$OE1^{E47}$	2.8	2.5	$OE1^{E114}$	2.3	2.4	H_2O	2.4	ND
	$OE2^{E47}$	2.6	2.8	$OE2^{E114}$	2.5	2.8			

[a] des3-20, Ca^{2+}-bound form of des3-20ALG-2.
[b] Full, Zn^{2+}-bound form of ALG-2.

between antiparallel helices (α7 and α8). Small conformational changes by Ca^{2+} are common to the crystal structures of PEF proteins. Nevertheless, greater changes are observed in the EF1 region of calpain dVI (Blanchard et al., 1997) and grancalcin (Jia et al., 2001a). Comparison of the structure of the Ca^{2+}-bound form (magenta) and that of the Zn^{2+}-bound form (green) with that of the Ca^{2+}-free form (cyan) reveals little difference in EF1 (Figure 2A), whereas there is 2.4 Å movement (Ca^{2+}-bound form) or 2.1 Å movement (Zn^{2+}-bound form) of Phe122 C^{α} in α5 by superimposing the first helix in EF3 (Figure 2B). On the other hand, while 3.5 Å movement of Phe188 C^{α} in α8 was observed in the Ca^{2+}-bound structure, little movement was observed in the Zn^{2+}-bound structure (Figure 2C). Thus, the structure of EF5 in the Zn^{2+}-loaded ALG-2 crystal resembles the structure of EF5 in the Ca^{2+}-free des3-20ALG-2 crystal, reflecting the absence of EF-hand-type coordination of Zn^{2+} in EF5 (Table 1).

As previously shown in the structure of Ca^{2+}-bound mouse ALG-2 (Jia et al., 2001b), human ALG-2 homodimers also form large crevices between each monomer molecule (molecules A and B) (Figure 2D). Alignment of each molecule A at α7 caused a greater shift of molecule B in the Ca^{2+}-bound form (magenta) than in the Zn^{2+}-bound form (green) when compared with the Ca^{2+}-free form (cyan). This is due to the effect of Ca^{2+} on EF5 structure. Although ALG-2 exhibits small Ca^{2+}-induced conformational changes, fluorescence photometric analyses previously revealed that binding of Ca^{2+} to ALG-2 induces exposure of hydrophobic surfaces (Maki et al., 1998; Lo et al., 1999; Tarabykina et al., 2000; Subramanian et al., 2004). Rearrangements of side chains of residues from Phe122 to Arg125 may account for the results of fluorescence analyses (see subsequent discussion).

Structure of ALG-2/Alix ABS Peptide Complex

We attempted cocrystalization of ALG-2 with a 16 residue peptide of the ALG-2 binding site (ABS) in Alix (corresponding to 799–814, Cys813 substituted with Ser to avoid oxidization; Figure 1) in the presence of Ca^{2+}, but good crystals were not obtained. Instead, we cocrystallized des3-23ALG-2 with the 16 residue Alix ABS peptide in the presence of Zn^{2+} and solved the

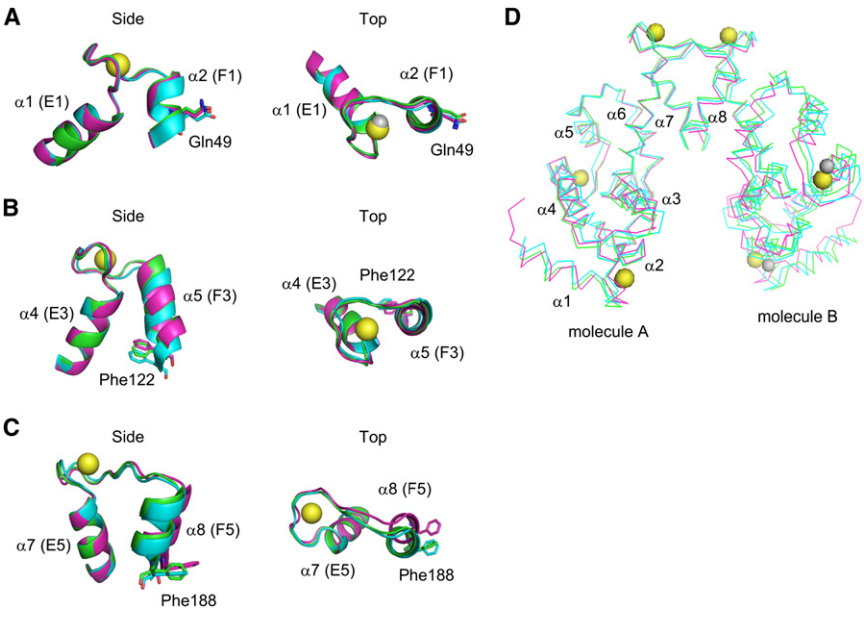

Figure 2. Comparison of Ca^{2+}-Free and Ca^{2+}-Bound Forms and Zn^{2+}-Bound Form of ALG-2

(A–C) Structures of EF1 (A), EF3 (B), and EF5 (C) of Ca^{2+}-free form (cyan) and Ca^{2+}-bound form (magenta) of des3-20ALG-2 and Zn^{2+}-bound form (green) of full-length ALG-2 are superimposed and shown in ribbon representation in side views and top views by aligning helices of (A) α1 (E1), (B) α4 (E3), and (C) α7 (E5), respectively, with the secondary structure matching program in COOT. Calcium atoms and zinc atoms are shown as yellow spheres and gray spheres, respectively.

(D) Overall structures of dimeric ALG-2 molecules in the three forms are aligned at α7 of molecule A and shown in wire presentation. The N-terminal Gly/Pro-rich region is invisible.

structure at 2.2 Å resolution (PDB code 2ZNE). Metal coordination of des3-23ALG-2 was the same as that of full-length ALG-2 in the Zn^{2+}-bound form (PDB code 2ZN8). An asymmetric unit of the crystal contains two ALG-2 molecules (A and B) as a dimer, but, surprisingly, each ALG-2 molecule binds the Alix ABS peptide in a different manner: molecule A binds one Alix ABS peptide (C), whereas molecule B binds two partial Alix ABS peptides (D and its crystallographic symmetry mate, D′). While peptide C binds only molecule A, peptide D (and also peptide D′) binds both molecules B and B′, which are related by crystallographic two-fold symmetry (Figure 3A). The Alix ABS peptides are seen in a groove composed of residues from the end of α3 to the middle of the loop between α7 and α8 (Figure 3B). The groove of ALG-2 contains two distantly positioned peptide binding pockets (pockets 1 and 2). Pocket 1 is formed by residues of the α5-α6 loop and those from EF5 (from α7 to α8). Pocket 2 is formed by residues from α3, α4, α5, and α7.

Hydrophobic interactions and hydrogen bonds between ALG-2 molecules and Alix ABS peptides are summarized in Figure 3C and in Table S2. All residues of peptide C, except for the first one, are visible in the crystal. Residues 7-TYPG-10 and 14-YS-15 of peptide C do not interact with ALG-2 molecule A (Figure 3D), but they are involved in intramolecular interactions (Table S3); in addition, residues 7-TYPG-10 are involved in crystal packing with molecule B (data not shown). The N-terminal part (2-GPPYP-6) of peptide C, designated as site 1, binds pocket 1, whereas the C-terminal part (11-YPG-13 and Q16) of peptide C, site 2, binds pocket 2 of molecule A (Figure 3D). In the case of peptide D, the last four residues, 13-GYSQ-16, are invisible. The N-terminal 2-GPPYP-6 (site 1) of peptide D binds pocket 1 of molecule B (Figure 3E). The C-terminal part of peptide D comes off molecule B and goes toward the neighboring molecule B′, and 8-YPGYPG-12 of peptide D, designated as site 3, binds pocket 2 of molecule B′. Symmetrically, pocket 2 of molecule B accommodates site 3 of peptide D′.

The binding mode of the N-terminal part of the Alix peptide (2-GPPYP-6; site 1) by pocket 1 of ALG-2 is almost identical in both molecules of the dimer (Figures 3D and 3E and Figure S4 and Table S2). The side chain of R125 of ALG-2 blocks the groove between the α5-α6 loop and the α7-α8 loop to complete pocket 1. The peptide side chains of P3, P4, and P6 pack against the α7-α8 loop, R125 side chain, and the α5-α6 loop, respectively. The Y180 side chain from the counterpart molecule constitutes the bottom of pocket 1 and accommodates the side chains of peptides P4 and Y5. On the other hand, the binding mode of the C-terminal part of the Alix peptide by pocket 2 of ALG-2 shows significant differences between two molecules of the dimer. When ALG-2 molecules A and B are superimposed, P12 of peptide C and P9 of peptide D′ occupy the same position in pocket 2, stacking against the side chain of W95 of ALG-2. The Y11 residue of peptide C and Y8 residue of peptide D′ are accommodated in almost the same position of pocket 2; however, their side chains show different orientations. These YP residues would be the consensus binding motif for pocket 2. The conformation of peptides C terminal to this YP motif largely differs between peptide C and D′. The backbone of peptide C folds back at G13 against pocket 2, and Y14 and S15 do not interact with ALG-2. The side chain of Y14 faces against P9 intramolecularly (Table S3). On the other hand, 10-GYP-12 of peptide D′ extends along the surface of pocket 2 (Figure 3E).

Critical Residues in Alix and ALG-2 for Their Binding

To determine the contributions of individual amino acid residues in Alix to interaction with ALG-2, we performed in vitro overlay binding assays of various alanine-substituted GST-AlixABS-His mutants (Figure 4A) with biotin-labeled ALG-2 (bio-ALG-2) as a probe and GST-His as a negative control. As shown in Figure 4B, bio-ALG-2 binding signals were lost or significantly reduced in the mutants at site 1, whereas mutations at sites 2 or 3 had smaller effects. Substitutions into glycines instead of alanines at P9 and P12 had similar partial effects on binding abilities (data not shown). Next, we investigated whether the mutations at site 1 were also crucial in the full-length Alix protein to interact with ALG-2. Green fluorescent protein-fused Alix (GFP-Alix) of wild-type (WT) and mutants (P802A, Y803A, and P804A, corresponding to P4A, Y5A, and P6A, respectively) were transiently expressed in HEK293T cells, and the proteins that were immunoprecipitated with an anti-GFP antibody were separated by SDS-PAGE, transferred to PVDF membranes, and then analyzed by Western blotting (Figure 4C, left panel) and bio-ALG-2 overlay assay (right panel), in which GFP served as a negative control. Signals of the mutants were significantly reduced compared with those of the WT, and only faint bands were observed.

Critical residues in ALG-2 were also investigated by GST-pull-down assay. Substitutions of residues that make contact with peptide C at site 1 in pocket 1 of ALG-2 (Y124, R125, D169, and Y180) resulted in loss of binding abilities (Figure 4D). Among the residues in pocket 2, the binding abilities were lost by mutations of Y91 and W95, but augmented by mutations of M71 and Q159. The alternatively spliced isoform, ALG-$2^{\Delta GF122}$, lacks the ability to bind Alix, in agreement with previous reports (Tarabykina et al., 2000; Shibata et al., 2007, 2008). Deletion of F122 causes a significant decrease in binding to Alix, as determined by SPR analysis (Subramanian et al., 2004). The side chain of F122 interacts with Y11 of Alix peptide C, and carbonyl carbon of G123 interacts hydrophobically with P6 C^{δ} of peptide C (Table S2), suggesting importance of these residues for Alix peptide binding.

Ca^{2+}/EF3-Driven Configuration Change of Arg125 Side Chain

To understand in detail the structural basis for Ca^{2+}-dependent binding of ALG-2 to Alix ABS peptide, we compared the three elucidated ALG-2 structures. Since site 1 is common to peptide C (in molecule A) and peptide D (in molecule B) or D′ (in molecule B′), and the 3-PPYP-6 sequence is critical for ALG-2 binding (Figure 4B), we analyzed Ca^{2+}-dependent rearrangements of residues in Pocket 1 (Figure 5A, left panel, green). This hydrophobic pocket becomes open upon binding of Ca^{2+} to EF3, exposes Y180 from molecule B (Figure 5B, left panel, aquamarine), and makes contact with 3-PPYP-6 (Figure 3D). The side chain of R125 is exposed to a solvent, and its electron density is low in the Ca^{2+}-free form, suggesting flexibility of the residue. Upon Ca^{2+} binding, the guanidino nitrogen atom of R125 forms a hydrogen bond with the peptide carbonyl oxygen atom of S120 (distance, 2.8 Å) in such a way that the R125 side chain becomes stabilized (Figure 5B, right panel). Moreover, an increase in the distance between Y124 C^{ζ} and L158 C^{γ} is observed (3.7 Å in the Ca^{2+}-free structure and 4.5 Å in the Ca^{2+}-bound structure). Upon Alix ABS peptide binding, pocket 1 is reclosed by the

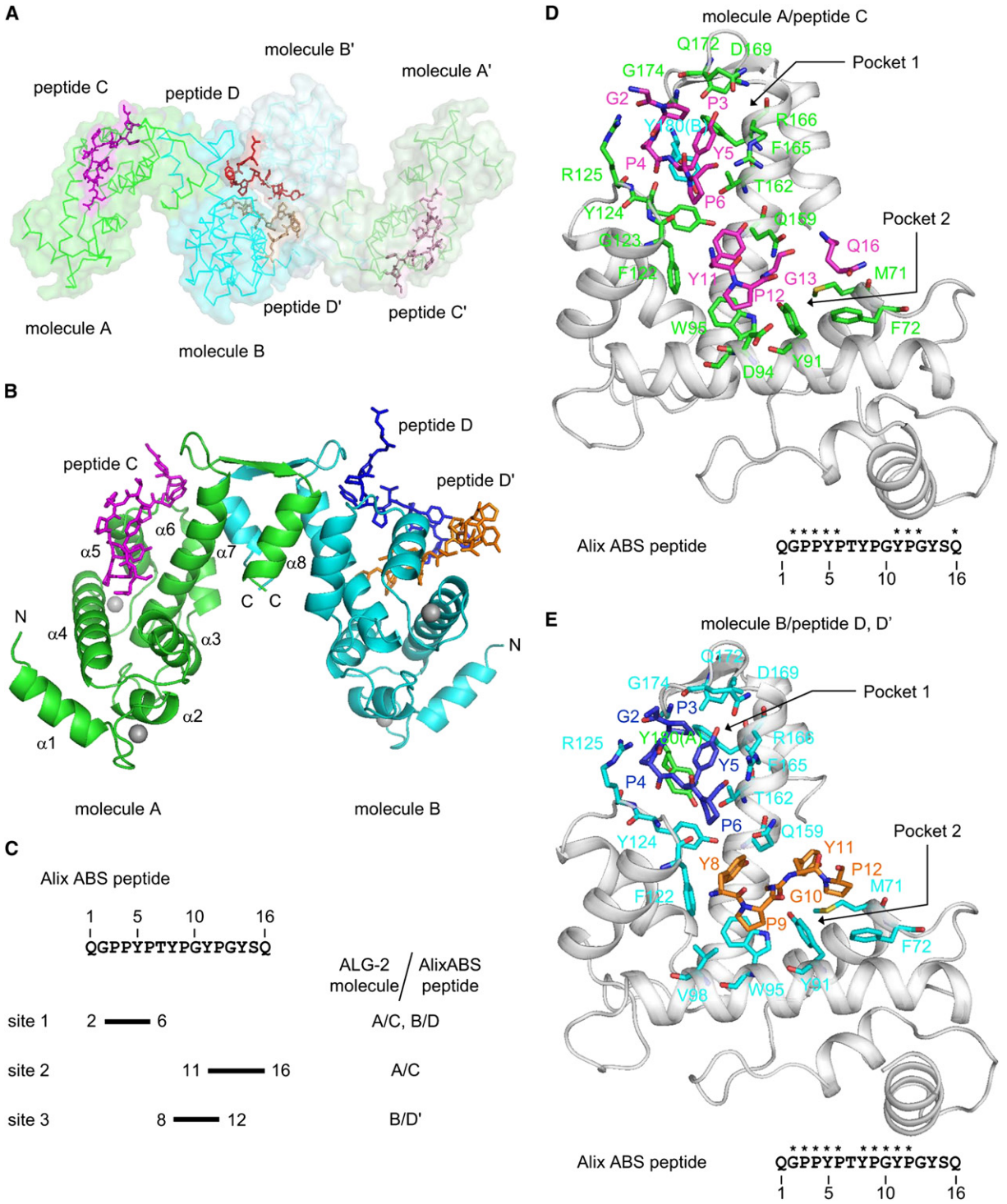

Figure 3. Crystal Structure of ALG-2/Alix ABS Peptide Complex

(A) Structure of two-fold symmetric ALG-2 tetramer (molecules A, A′, B, and B′) complexed with four peptide molecules with two different binding patterns (peptides C, C′, D, and D′) is shown in wire representation of ALG-2 C^{α}, as well as superimposed transparent surface representation in green for molecule A and cyan for molecule B, respectively. Peptides are shown in stick representation and colored magenta for peptide C and red for peptide D.

(B) Two monomers (molecules A and B) are shown in green and cyan in ribbon representation, respectively. The peptides are shown in magenta (peptide C), blue (peptide D), and orange (peptide D′). EF-hand-coordinated zinc atoms are shown as gray spheres.

(C) Summary of ALG-2/peptide contact sites.

(D and E) Ribbon diagrams of the ALG-2/Alix ABS peptide complex in the monomeric ALG-2 molecule and stick representation of interacting residues. Carbon atoms in ALG-2 molecules and Alix peptides are shown and colored similarly to (B). Carbon atoms of Y180 from the counter ALG-2 molecule are colored cyan (D)

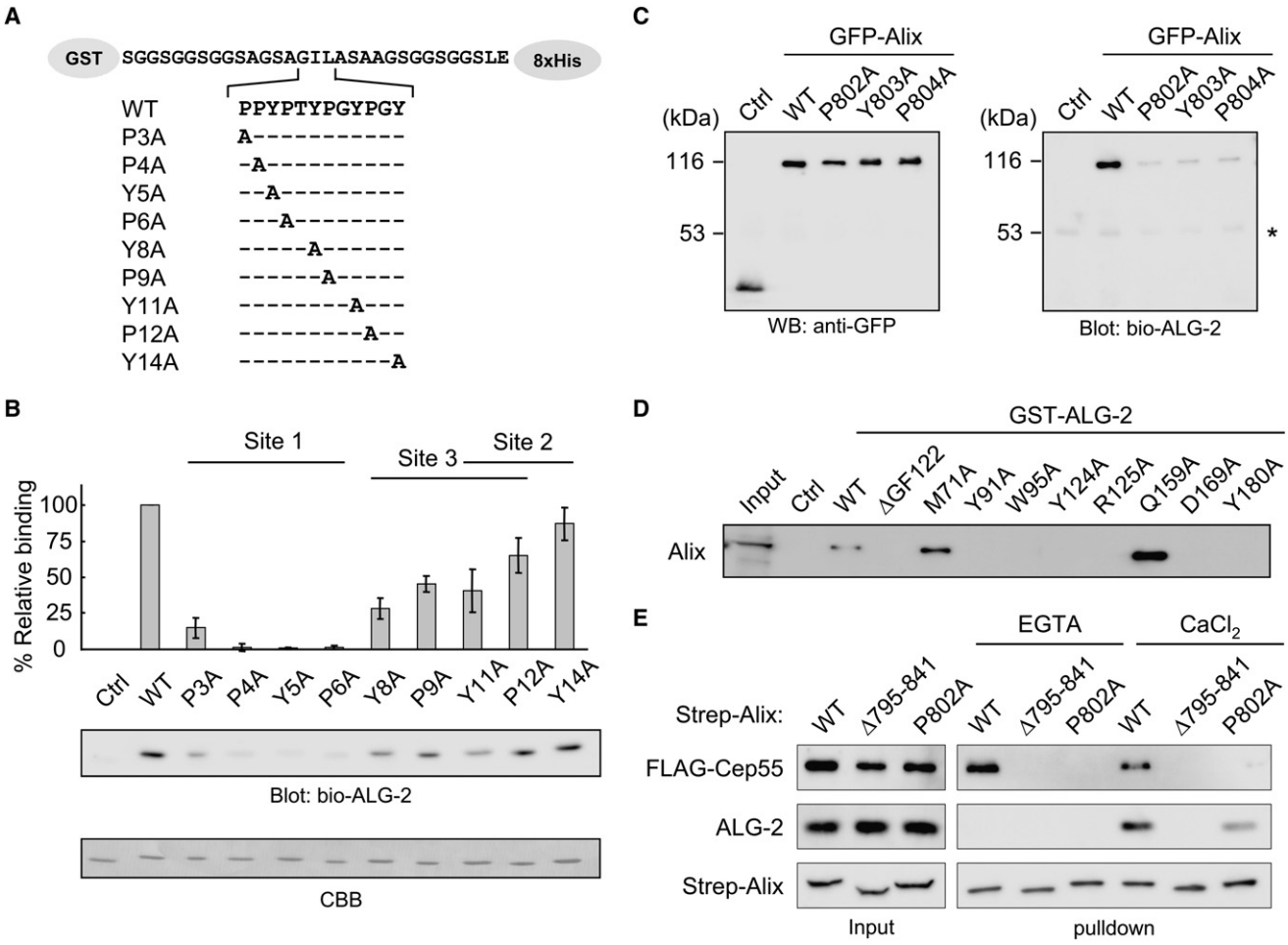

Figure 4. Mutational Analyses of Interactions between ALG-2 and Alix Peptide

Critical residues for interactions between ALG-2 and Alix were identified by site-specific mutagenesis.

(A) Alanine-scanning mutants of GST-fused Alix peptide were generated by inserting into a GST-His expression vector (control) each synthetic oligonucleotide block encoding residues 3–14 of the Alix ABS peptide in which each Pro and Tyr was substituted with Ala.

(B) Purified proteins were subjected to overlay assay with bio-ALG-2. Relative binding abilities compared to WT were calculated and expressed in percentages. The values obtained from triplicate experiments are expressed as means ± SD. A representative result is shown for the blot. CBB, Coomassie Brilliant Blue staining.

(C) GFP-fused full-length Alix proteins of WT and amino acid-substituted mutants were expressed in HEK293T cells and subjected to Western blotting (WB) (left panel) and bio-ALG-2 overlay assay (right panel) after immunoprecipitation with anti-GFP antibody. Unfused GFP was used as a negative control (Ctrl). Nonspecific signals derived from IgG heavy chain are indicated by an asterisk.

(D) Endogenous Alix protein in HEK293 cells was pulled down with GST-fused WT, alternatively spliced isoform (ΔGF122), and single amino acid-substituted mutants of ALG-2, as described in Experimental Procedures. Unfused GST was used as a negative control (Ctrl). Proteins bound to glutathione Sepharose beads (pull-down products) were subjected to Western blotting with anti-Alix antibody. Input, 15%. (E) HEK293T cells were cotranfected with expression vectors for Strep-tagged Alix of either WT, Δ795-841, or P802A mutant and FLAG-Cep55. Cleared lysates were subjected to pull-down assay with Strep-Tactin beads in the presence of 5 mM EGTA or 100 μM $CaCl_2$. Proteins in the cleared lysates (input) and those bound to the beads (pull-down products) were analyzed by Western blotting with anti-FLAG monoclonal antibody (mAb), anti-Strep mAb and anti-ALG-2 polyclonal antibody, respectively.

side chain of R125 (Figure 5C). Taken together, the Ca^{2+}-dependent binding of ALG-2 to Alix ABS peptide is explained as shown in Figure 6: (1), change in geometry of helices E3 and F3 cause detachment of the Y124 side chain from L158; (2) change in configuration of the R125 side chain; (3) opening of pocket 1; (4) entry of the peptide; and (5) half closure of pocket 1 by the R125 side chain and completion of the peptide trapping. Thus, R125 is a key element of the open-close mechanism of pocket 1, and acts as a switch driven by Ca^{2+}/EF3 conformational change.

and green (E). Other atoms are also colored: nitrogen, blue; oxygen, red. The ALG-2 molecule is shown in gray in ribbon representation. Residues of Alix ABS peptide that are involved in interaction with ALG-2 are indicated by asterisks above the sequence: (D) molecule A/peptide C; (E) molecule B/peptides D and D′. Arrows indicate hydrophobic pockets (pockets 1 and 2).

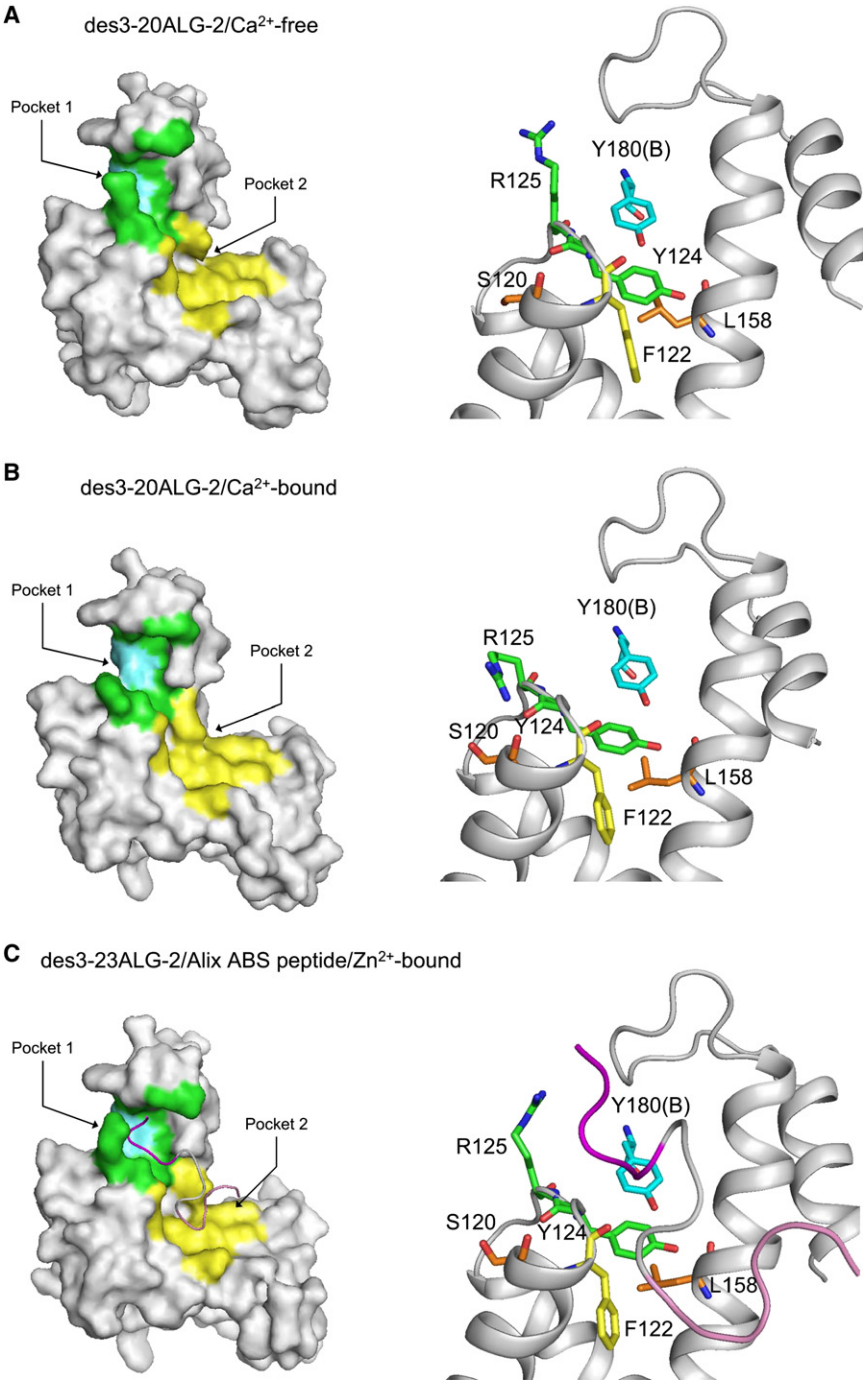

Figure 5. Structural Basis for Ca^{2+}-Dependent Binding of Alix Peptide to ALG-2

Structures of (A) Ca^{2+}-free des3-20ALG-2, (B) Ca^{2+}-bound des3-20ALG-2, and (C) Alix peptide C complex of des3-23ALG-2 coordinated with Zn^{2+} are compared. Left panels: surface representation of molecule A. Residues of ALG-2 that hydrophobically interact with Alix peptide C at sites 1 and 2 are colored green (G123, Y124, R125, T162, F165, Q172, G174) (pocket 1) and yellow (M71, F72, Y91, D94, W95, F122, Q159) (pocket 2), respectively. Y180 from molecule B is colored aquamarine. Alix ABS peptide is shown in ribbon representation, and sites 1 and 2 are colored magenta and pink, respectively, in (C). Right panels: close-up views of pocket 1 and its vicinity are shown in ribbon representation and in the stick models for critical residues involved in opening of pocket 1 or binding with Alix ABS peptide. Carbon atoms are colored green for site 1 acceptor residues (Y124 and R125), yellow for a site 2 acceptor residue (F122), and orange for signal transducing residues (L158 and S120). Carbon atoms of Y180 from molecule B are colored in cyan. Oxygen atoms and nitrogen atoms are in red and blue, as indicated.

Comparison with Published Structure of Ca^{2+}-Bound Mouse des1-20ALG-2

As shown in Figure S5, the configuration of R125 is significantly different between the structure of human des3-23ALG-2/Alix ABS peptide complex and the previously published structure of mouse ALG-2 by Jia et al. (2001b) (PDB code 1HQV), in which des1-20ALG-2 was thought to capture an N-terminal clipped decapeptide 8-PGPGGGPGPA-17 that was obtained after elastase treatment of full-length ALG-2. Hydrogen bonds and hydrophobic interactions are detected between R125 and Alix ABS peptide (G2 and P4), and mutation of R125 to alanine caused a loss of binding ability to Alix (Figure 4D). On the other hand, P8 and P10 of the N-terminal ALG-2 decapeptide, positioned similarly to G2 and P4 of Alix peptide in pocket 1, are placed beyond the bonding distance from R125 in 1HQV. Moreover, guanidino group nitrogen of R125 forms a hydrogen bond with carbonyl oxygen of S120, as in the case of the Ca^{2+}-bound but peptide-free structure of human des3-20ALG-2 (Figure 5B).

Jia et al. (2001b) previously crystalized the Ca^{2+}-bound form of mouse des1-20ALG-2 with a buffer containing polyethylene glycol (PEG) 8000 after treatment of full-length recombinant ALG-2 with elastase. They found a continuous electron density in a hydrophobic groove in the solved ALG-2 structure, and interpreted it as a Gly/Pro-rich decapeptide derived from the cleaved N-terminus. We also crystalized ALG-2 in the presence of PEG8000, but with genetically engineered N-terminally truncated des3-20ALG-2. Surprisingly, we observed an electron density in a similar hydrophobic groove in each ALG-2 monomer (molecules A and B) in the asymmetric unit (Figure S6). Mass spectrometric analyses of the purified recombinant des3-20ALG-2 protein did not show significant signals in the 750–10,000 Da range (data not shown), suggesting that no bacterial peptides were captured during purification. By interpreting the continuous electron density as a portion of PEG8000 molecule, we constructed a structural

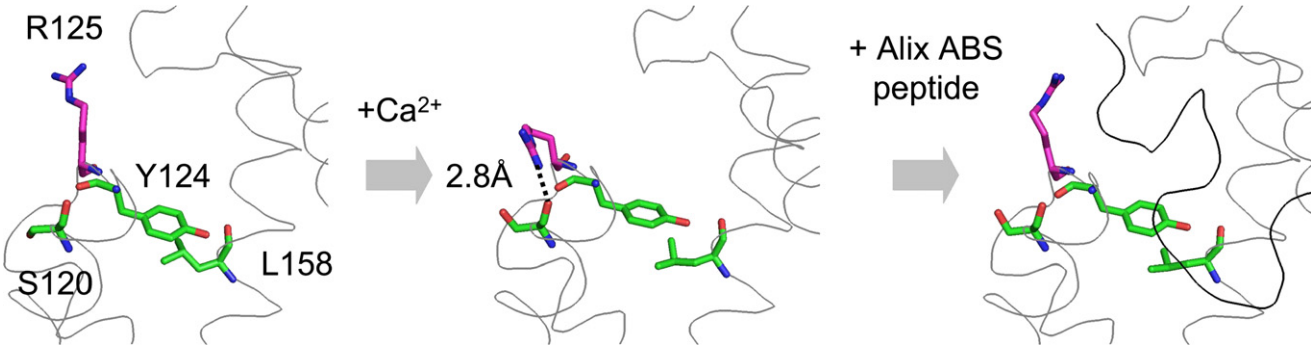

Figure 6. Model of Ca^{2+}/EF3-Driven Arginine Switch Mechanism

A proposed model of the arginine switch mechanism for Ca^{2+}-dependent binding of ALG-2 to its target peptide. Left panel: In the Ca^{2+}-free form, the flexible side chain of R125 blocks the mouth of the hyrophobic groove and interferes with entry of the target peptide. Middle panel: upon binding of Ca^{2+} to EF3, the side chain of Y124 detaches from L158 and the guanidino nitrogen atom of R125 forms a hydrogen bond with the carbonyl oxgen atom of S120 in the distance of 2.8 Å, resulting in opening of the hydrophobic pocket. Right panel: a target peptide enters the pocket and is anchored there by interacting hydrophobically with Y124 as well as with side chain carbon atoms of R125, resulting in a partial closure of the pocket. In stick representation, atoms of amino acid residues involved in the arginine switch model are colored as follows: carbon, green for S120, Y124, and L158, and magenta for R125; oxygen, red; nitrogen, blue. Wire and ribbon represent the main chain in gray and Alix ABS peptide in black, respectively.

model of conjugated ethylene glycol oligomer, $HO(CH_2CH_2O)_nH$, residing in the hydrophobic groove including pockets 1 and 2 (molecule A, n = 9; molecule B, n = 11) (PDB code 2ZN9). However, we cannot exclude the possibility that the hydrophobic cleft has a capacity to hold flexible hydrophobic peptides, including the N-terminal region of ALG-2, with a low affinity. A higher tendency of Ca^{2+}-dependent aggregation of full-length ALG-2 than N-terminal deleted ALG-2 at high concentrations of the ALG-2 proteins (Maki et al., 1998; Figures S2C–S2F) may be explained by intermolecular interactions between the N-terminal segment and the hydrophobic pockets.

Comparison with Other PEF Proteins

Although crystal structures of PEF family members have been accumulating, comprehensive comparison between ALG-2 and other PEF proteins has not been done yet. In the present study, it became possible to compare homodimers of ALG-2 and calpain dVI (PEF domain of small subunit) in three forms: Ca^{2+}-free form, Ca^{2+}-bound form, and peptide-bound form. As shown in Figure 7 and in Figure S7, difference in overall structures between ALG-2 and calpain dVI in each form becomes apparent when antiparallel loops of EF5s (magenta) are placed horizontally and compared with each other from three different views (top, side, and bottom): (1) when projected onto the paper surface (X-Y plane), the position of EF1 (cyan) relative to EF3 (green) is less rotated around the two-fold symmetric axis in ALG-2 than in calpain dVI, counterclockwise in top view and clockwise in bottom view, respectively; (2) the ALG-2 dimer has a large crevice and less interacting surface between the two monomer molecules (calculated surface area buried at interface: ALG-2/Ca^{2+}, 2849 $Å^2$; calpain dVI/Ca^{2+}, 4225 $Å^2$); and (3) Alix ABS peptide binds to a hydrophobic groove formed by residues from EF2 to EF5 in ALG-2 (top view and side view), whereas calpastatin domain 1C peptide in an α-helical conformation binds to a groove formed by EF1 and a hydrophobic surface along F2E3 (side view and bottom view). The binding surfaces for these peptides partly coincide with the area of Ca^{2+}-induced conformational rearrangement in helix F3 and F3E4 loop in ALG-2 (Figures 2, 5, and 6) and EF1 in calpain dVI (Blanchard et al., 1997), respectively.

Regarding three-dimensional structures of grancalcin, the Ca^{2+}-free (apo) form and the form of Ca^{2+}-bound at EF1 and EF3 have been solved (Jia et al., 2001a). Superimposition of both forms of grancalcin (red) with the respective form of ALG-2 (blue) at α7 helices shows a different arrangement of EF1/EF2 relative to EF5 (Figure S8). Relative positions of EF3/EF4 segments in ALG-2 and grancalcin differ more in the Ca^{2+}-free forms than in the Ca^{2+}-bound forms. The critical switch-acting R125 in ALG-2 is conserved in grancalcin (R154) and sorcin (R135), but not in other human PEF proteins (peflin, N216; μ-calpain large subunit, K650; calpain small subunit, H204). Comparison of the configuration of the side chain of R154 in grancalcin between their structures of the Ca^{2+}-free and Ca^{2+}-bound forms shows that conformational movement is opposite to ALG-2 (Figures 5 and 8). Guanidino group nitrogen of R154 in grancalcin forms a hydrogen bond with carbonyl oxygen of G149 in the Ca^{2+}-free form, and this latch is released in the Ca^{2+}-bound form. Interestingly, grancalcin associates with L-plastin, but the complex dissociates in the presence of Ca^{2+} (Lollike et al., 2001). It remains to be established whether this Ca^{2+}-dependent negative regulation of the interaction between grancalcin and L-plastin is related to the Ca^{2+}/EF3-driven arginine switch mechanism proposed in the present study.

Regarding crystal structures of sorcin, only Ca^{2+}-free forms have been solved (Xie et al., 2001; Ilari et al., 2002). The side chain configuration of sorcin R135 is not fixed due to greater B factors (>70). Results of site-directed mutagenesis and a variant protein suggest that sorcin is activated upon Ca^{2+} binding to EF3 and transmission of the conformational change at its loop via the D helix (α4 helix) to EF2, and from there to EF1 via canonical structural/functional pairing (Mella et al., 2003). Interestingly, W105 in sorcin, which is located in the D helix and corresponds to W95 in ALG-2, was found to be important for binding to annexin A7 (Colotti et al., 2006). Substitution of W95 in ALG-2 with alanine also caused a loss of the binding ability to annexin A7 (Shibata et al., 2008) as well as Alix (Figure 4D). Although there

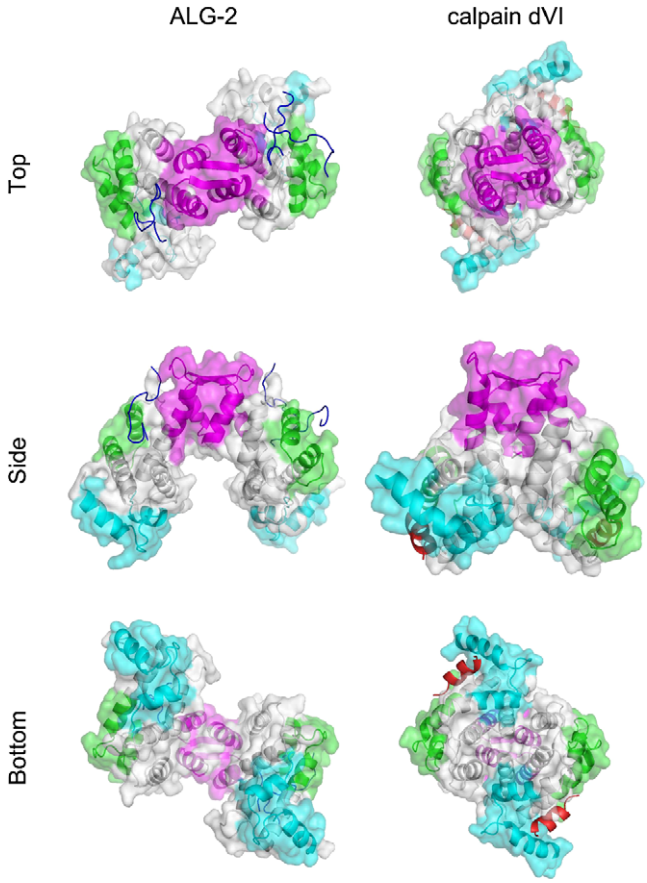

Figure 7. Structural Comparison between ALG-2 and Calpain dVI in Peptide Complex Forms

Dimeric structures are compared between ALG-2 and the PEF domain of calpain small subunit (dVI) in the complex with respective target peptide (ALG-2/Zn^{2+}/Alix peptide, present study; calpain dVI/Ca^{2+}/calpastatin peptide, Todd et al., 2003). Structures are represented in transparent surface superimposed with ribbon representation. EF1, cyan; EF3, green; EF5, magenta; Alix ABS peptide, blue; calpastatin domain 1C peptide, red. Symmetric two-fold axes of PEF dimers are perpendicular to the paper surface in top view and bottom view.

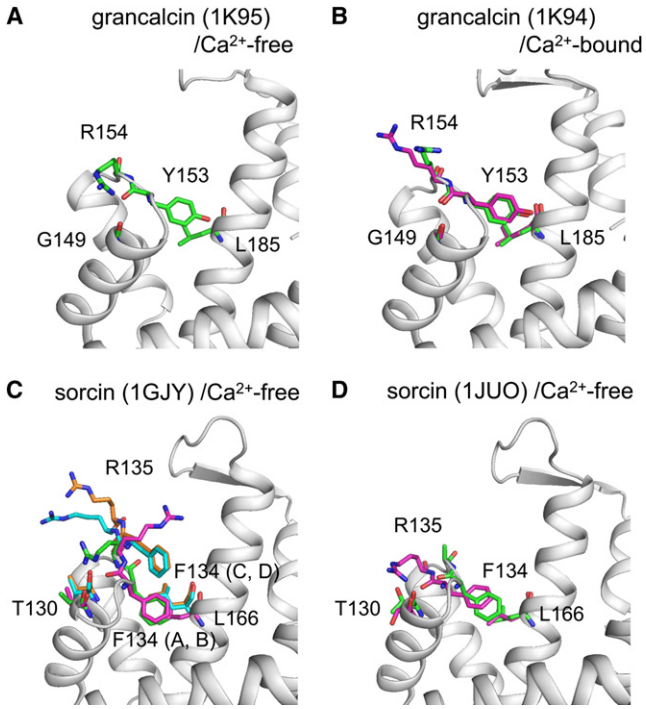

Figure 8. Side Chain Configuration of Conserved Arginine in the F3-E4 Loop of Grancalcin and Sorcin

In the proposed arginine switch model of ALG-2, three other residues (S120, Y124, and L158) are involved in addition to R125. Configurations of the corresponding residues in grancalcin ([A] Ca^{2+}-free form, PDB code 1K95; [B] Ca^{2+}-bound form, 1K94) and in sorcin ([C and D] Ca^{2+}-free form; C, 1GJY; D, 1JUO) are shown. Atoms are colored red, oxygen; blue, nitrogen. Carbons in molecule A, green; molecule B, magenta; molecule C, aquamarine; molecule D, orange. Side chain of R135 in molecule A of sorcin in 1JUO is invisible.

is coincidence in the importance of W95 in ALG-2 and corresponding W105 in sorcin for annexin A7 binding, the detailed mode of binding may be different for the two PEF proteins, because the N-terminal Gly/Pro-rich region is dispensable for ALG-2 (Satoh et al., 2002b), but essential for sorcin (Verzili et al., 2000).

ALG-2 Binding Motif

Although exact binding sites are not yet known, several other ALG-2-binding proteins also contain sequences rich in Pro, Gly, and Tyr, such as annexin A7 (4-PGYPPTGYPP-15), annexin A11 (4-PGYPPPPGGYPP-15), and TSG101 (188-CPYPPGGP YPA-198), suggesting a consensus sequence PPYP(X_{3-5})YP (where *X* is uncharged amino acid). Optimum sequence and number of residues between two YPs may depend on surrounding residues. Sec31A and Scotin, however, do not conform to this sequence, but they also contain a segment rich in Pro and Tyr, such as 869-PPYPQPQPYQP-877 in Sec31A and 190-PYPMQYPPP YP-200 in Scotin, respectively. Recently, we identified two different types of ABSs in the N-terminal Pro-rich region of phospholipid scramblase 3: Alix type, 8-KGYAPSPPPPYPVTPGYPE PA-28, and non-Alix type, 41-QVPAPAPGFALFPSPGPVA-61 (Shibata et al., 2008). While the Alix-type sequence binds to ALG-2 but lacks the ability to bind ALG-$2^{\Delta GF122}$, the non-Alix type binds to both isoforms of ALG-2. Sec31A also binds to ALG-$2^{\Delta GF122}$ (Shibata et al., 2007), but its binding site has not been identified yet. ALG-2 may present flexible binding surfaces to various proteins with broad specificities and different affinities, and probably even to PEG.

Recently, Cep55 (centrosome protein 55 kDa) was reported to bind both Alix and TSG101 and to regulate cytokinesis by recruiting ESCRTs (Carlton and Martin-Serrano, 2007; Morita et al., 2007; Carlton et al., 2008). The proposed Cep55-recognition sequence in Alix, 800-GPP-802, partially overlaps with the ALG-2-binding motif. As shown in Figure 4E, the single amino acid substitution mutant of Alix P802A abrogated FLAG-Cep55 binding, and significantly reduced ALG-2 binding by the pull-down assay with Strep-Alix expression constructs. The presence of Ca^{2+} in the binding buffer caused a slight decrease in FLAG-Cep55 binding compared with the presence of EGTA, but the degree of the decrease seems to be dependent on levels of exogenously expressed FLAG-Cep55 and Strep-Alix in the repeated experiments (data not shown). Although further investigation is

necessary to evaluate the effect of Ca^{2+} on the binding efficiency of Cep55, ALG-2 may play a role as an auxiliary factor in regulating biological functions in which Alix and ESCRTs are required in conjunction with Ca^{2+} signaling.

In conclusion, in the present study, we have clarified the structural basis for the Ca^{2+}-dependent binding of ALG-2 to Alix by crystal structural analyses. Compared with other PEF proteins described above (Figure 7; Figures S7 and S8) and with calmodulin (Supplemental Results and Discussion), ALG-2 has a unique activation mechanism. Binding of Ca^{2+} to EF3 induces rearrangement of R125 present in the loop connecting EF3 and EF4, and makes a hydrophobic pocket accessible to PPYP, the primary binding site of Alix peptide. We propose a Ca^{2+}/EF3-driven arginine switch mechanism.

EXPERIMENTAL PROCEDURES

Expression Plasmids

Bacterial expression of N-terminally truncated human ALG-2 that lacks the Gly/Pro-rich region, designated ALG-2ΔN23, was described previously (Satoh et al., 2002a), and this protein is renamed des3-23ALG-2 here. Construction of an expression plasmid of des3-20ALG-2 and point mutations of the expression plasmids for GST-ALG-2 and GFP-Alix were performed with a QuikChange Site-Directed Mutagenesis kit (Stratagene, USA). A control expression plasmid of GST-His containing two flexible GGS linkers between GST and multiple cloning site and between multiple cloning site and 8× His, designated pGST-His, was constructed by inserting two pairs of double-stranded oligonucleotides into pET42b(+) (Invitrogen) by two-step insertions: first step: 5′-CTAGTGGT GGCTCAGGTGGTTCTGGTGGCTCAGCCGGTTCGGCAGG-3′ and 5′-AATTC CTGCCGAACCGGCTGAGCCACCAGAACCACCTGAGCCACCA-3′ into the *Spe*I/EcoRI site; second insertion: 5′-AATTCTTGCCTCGGCGGCAGGTTCAG GTGGTTCTGGTGGCTCAC-3′ and 5′-TCGAGTGAGCCACCAGAACCACCTG AACCTGCCGCCGAGGCAAG-3′ into the SmaI/HindIII site. GST-fusion proteins containing the ALG-2 binding sequence and its mutant sequences were constructed by inserting double-stranded oligonucleotides into the BglII-digested larger fragment of pGST-His.

Purification of Recombinant ALG-2 Proteins and GST-Fused Alix Peptides

For X-ray crystallographic analyses, ALG-2 or deletion mutant ALG-2 proteins were expressed and purified essentially as described previously with an affinity column immobilizing an ALG-2 binding oligopeptide of phospholipid scramblase 3 (Shibata et al., 2008). Purified proteins were concentrated to about 10 mg/ml with a vacuum centrifuge evaporator (Sakuma, Japan). The concentrated proteins were dialyzed against 10 mM Tris-HCl, pH 7.5, containing 10 μM each of EDTA and EGTA. For GST pull-down assay, GST fusion proteins were expressed and purified with glutathione Sepharose beads (GE Healthcare) according to the manufacturer's instructions. For biotin-overlay assay, GST-His or GST-AlixABS-His proteins were purified first with TALON beads (Clontech) according to manufacturer's instructions, and then further purified with glutathione Sepharose beads.

Crystallization

All crystals, except for the divalent ion-free form of des3-20ALG-2, were grown by the sitting or hanging drop vapor diffusion method at 20°C. Full-length ALG-2 protein was crystallized with 25% (w/v) 2-methyl-2, 4-pentanediol (MPD), 100 mM sodium cacodylate, pH 6.5, and 75 mM zinc acetate. The Ca^{2+}-bound form of des3-20ALG-2 was crystallized with 18% (w/v) PEG8000, 100 mM sodium cacodylate, pH 6.5, and 200 mM calcium acetate. The Ca^{2+}-free form of des3-20ALG-2 was crystallized with 40% MPD, 100 mM Na_2HPO_4-KH_2PO_4, pH6.5, and 2 mM EDTA at 4°C, as described previously (Wu et al., 2001). The concentrated des3-23ALG-2 was added to the Alix peptide (Alix799-814: QGPPYPTYPGYPGYSQ, Cys813 substituted with Ser to avoid oxidization, purchased from Biosynthesis Inc., USA) with the protein-to-peptide molar ratio of 1:2 and crystallized with 10% (v/v) 2-propanol, 100 mM cacodylate, pH 6.5, and 200 mM zinc acetate.

Data Collection, Structure Determination, Refinement, and Analyses

All data were collected at beamlines BL-5A, 6A, and 17A of Photon Factory (Tsukuba, Japan) under cryogenic conditions with crystals soaked in a cryoprotectant solution containing 20% glycerol and cooled to 100K in a nitrogen gas stream. The diffraction data were integrated and scaled with the HKL2000 program package (Otwinowski and Minor, 1997). All crystal structures were solved by the molecular replacement method with the program MOLREP (Vagin and Teplyakov, 1997) with the structure of elastase-treated mouse ALG-2 (PDB code 1HQV) as a search model. All models were refined with the programs CNS (Brünger et al., 1998) and REFMAC5 (Murshudov et al., 1997). Manual adjustments of the model were performed with COOT (Emsley and Cowtan, 2004). All of the structural figures were generated with PyMol (DeLano Scientific LLC, Palo Alto, CA). Rmsd was calculated with the program CNS.

Bio-ALG-2 Overlay Assay and Pulldown Assays

Recombinant full-length ALG-2 was labeled with biotin in vitro with sulfosuccinimidyl *N*-(*D*-biotinyl)-6-aminohexanoate (Biotin-AC5 Sulfo-OSu) as described previously (Shibata et al., 2008). Overlay assay with bio-ALG-2 was performed essentially as described previously (Shibata et al., 2008), but modified by incubating the membranes with horseradish peroxidase-conjugated streptoavidin in TBS-T (20 mM Tris-HCl, pH 7.5, 150 mM NaCl, 1% Tween-20) containing 100 μM $CaCl_2$, 0.1% gelatin, 10 mM 2-mercaptoethernol and 1 mM $NiCl_2$ at 37°C for 1 hr. Signals were detected by the chemiluminescence method and analyzed with LAS-3000mini (Fuji Film, Tokyo, Japan). Inclusion of 1 mM $NiCl_2$ was found to be effective for suppressing nonspecific binding to GST-His protein (a negative control). For the detection of ALG-2 binding to full-length Alix WT and mutant proteins that were fused with GFP, GFP-Alix proteins were transiently expressed in HEK293T cells and immunoprecipitated with rabbit anti-GFP antiserum (Invitrogen), as described previously (Shibata et al., 2008), and then bio-ALG-2 overlay assay was performed as described above. GST pull-down assay for ALG-2 binding to endogenous Alix protein was performed as described previously (Shibata et al., 2008) with an anti-Alix polyclonal antibody (Shibata et al., 2007). A human Cep55 cDNA was obtained from OpenBiosystems and subcloned into a pCMV-Tag2B vector, and a pull-down assay with Strep-Alix was performed essentially as described previously (Ichioka et al., 2007).

ACCESSION NUMBERS

The atomic coordinates and structure factors have been deposited in the Protein Data Bank with accession codes 2ZND, 2ZNE, 2ZN8, and 2ZN9.

SUPPLEMENTAL DATA

Supplemental Data include eight figures, three tables, Supplemental Experimental Procedures, Supplemental Results and Discussion, and Supplemental References and can be found with this article online at http://www.structure.org/cgi/content/full/16/10/1562/DC1/.

ACKNOWLEDGMENTS

We thank Hitomi (Nagoya University), Kato (KEK), Narayana (UAB, USA), and Ichioka (Nagoya University) for valuable suggestions. This work was partly supported by a Grant-in-Aid for Scientific Research (B) (to M.M.) and a Grant-in-Aid for JSPS fellow (to H.S.) from JSPS.

Received: April 22, 2008
Revised: July 11, 2008
Accepted: July 24, 2008
Published: October 7, 2008

REFERENCES

Blanchard, H., Grochulski, P., Li, Y., Arthur, J.S., Davies, P.L., Elce, J.S., and Cygler, M. (1997). Structure of a calpain Ca^{2+}-binding domain reveals a novel EF-hand and Ca^{2+}-induced conformational changes. Nat. Struct. Biol. *4*, 532–538.

Brünger, A.T., Adams, P.D., Clore, G.M., DeLano, W.L., Gros, P., Grosse-Kunstleve, R.W., Jiang, J.S., Kuszewski, J., Nilges, M., Pannu, N.S., et al. (1998). Crystallography & NMR system: a new software suite for macromolecular structure determination. Acta Crystallogr. D Biol. Crystallogr. *54*, 905–921.

Carlton, J.G., and Martin-Serrano, J. (2007). Parallels between cytokinesis and retroviral budding: a role for the ESCRT machinery. Science *316*, 1908–1912.

Carlton, J.G., Agromayor, M., and Martin-Serrano, J. (2008). Differential requirements for Alix and ESCRT-III in cytokinesis and HIV-1 release. Proc. Natl. Acad. Sci. USA *105*, 10541–10546.

Colotti, G., Zamparelli, C., Verzili, D., Mella, M., Loughrey, C.M., Smith, G.L., and Chiancone, E. (2006). The W105G and W99G sorcin mutants demonstrate the role of the D helix in the Ca^{2+}-dependent interaction with annexin VII and the cardiac ryanodine receptor. Biochemistry *45*, 12519–12529.

Emsley, P., and Cowtan, K. (2004). Coot: model-building tools for molecular graphics. Acta Crystallogr. D Biol. Crystallogr. *60*, 2126–2132.

Hiraki, M., Kato, R., Nagai, M., Satoh, T., Hirano, S., Ihara, K., Kudo, N., Nagae, M., Kobayashi, M., Inoue, M., et al. (2006). Development of an automated large-scale protein-crystallization and monitoring system for high-throughput protein-structure analyses. Acta Crystallogr. D Biol. Crystallogr. *62*, 1058–1065.

Hosfield, C.M., Elce, J.S., Davies, P.L., and Jia, Z. (1999). Crystal structure of calpain reveals the structural basis for Ca^{2+}-dependent protease activity and a novel mode of enzyme activation. EMBO J. *18*, 6880–6889.

Ichioka, F., Takaya, E., Suzuki, H., Kajigaya, S., Buchman, V.L., Shibata, H., and Maki, M. (2007). HD-PTP and Alix share some membrane-traffic related proteins that interact with their Bro1 domains or proline-rich regions. Arch. Biochem. Biophys. *457*, 142–149.

Ilari, A., Johnson, K.A., Nastopoulos, V., Verzili, D., Zamparelli, C., Colotti, G., Tsernoglou, D., and Chiancone, E. (2002). The crystal structure of the sorcin calcium binding domain provides a model of Ca^{2+}-dependent processes in the full-length protein. J. Mol. Biol. *29*, 447–458.

Jang, I.K., Hu, R., Lacanà, E., D'Adamio, L., and Gu, H. (2002). Apoptosis-linked gene 2-deficient mice exhibit normal T-cell development and function. Mol. Cell. Biol. *22*, 4094–4100.

Jia, J., Han, Q., Borregaard, N., Lollike, K., and Cygler, M. (2000). Crystal structure of human grancalcin, a member of the penta-EF-hand protein family. J. Mol. Biol. *300*, 1271–1281.

Jia, J., Borregaard, N., Lollike, K., and Cygler, M. (2001a). Structure of Ca^{2+}-loaded human grancalcin. Acta Crystallogr. D Biol. Crystallogr. *57*, 1843–1849.

Jia, J., Tarabykina, S., Hansen, C., Berchtold, M., and Cygler, M. (2001b). Structure of apoptosis-linked protein ALG-2: insights into Ca^{2+}-induced changes in penta-EF-hand proteins. Structure *9*, 267–275.

Katoh, K., Suzuki, H., Terasawa, Y., Mizuno, T., Yasuda, J., Shibata, H., and Maki, M. (2005). The penta-EF-hand protein ALG-2 interacts directly with the ESCRT-I component TSG101, and Ca^{2+}-dependently co-localizes to aberrant endosomes with dominant-negative AAA ATPase SKD1/Vps4B. Biochem. J. *391*, 677–685.

Koch, M., Diez, J., and Fritz, G. (2008). Crystal structure of Ca^{2+}-free S100A2 at 1.6-Å resolution. J. Mol. Biol. *378*, 931–940.

Lin, G.D., Chattopadhyay, D., Maki, M., Wang, K.K., Carson, M., Jin, L., Yuen, P.W., Takano, E., Hatanaka, M., DeLucas, L.J., and Narayana, S.V. (1997). Crystal structure of calcium bound domain VI of calpain at 1.9 Å resolution and its role in enzyme assembly, regulation, and inhibitor binding. Nat. Struct. Biol. *4*, 539–547.

Lo, K.W., Zhang, Q., Li, M., and Zhang, M. (1999). Apoptosis-linked gene product ALG-2 is a new member of the calpain small subunit subfamily of Ca^{2+}-binding proteins. Biochemistry *38*, 7498–7508.

Lollike, K., Johnsen, A.H., Durussel, I., Borregaard, N., and Cox, J.A. (2001). Biochemical characterization of the penta-EF-hand protein grancalcin and identification of L-plastin as a binding partner. J. Biol. Chem. *276*, 17762–17769.

Maki, M., and Shibata, H. (2007). The penta-EF-hand protein ALG-2 and its interacting proteins. Calcium Binding Proteins *2*, 4–10.

Maki, M., Narayana, S.V., and Hitomi, K. (1997). A growing family of the Ca^{2+}-binding proteins with five EF-hand motifs. Biochem. J. *328*, 718–720.

Maki, M., Yamaguchi, K., Kitaura, Y., Satoh, H., and Hitomi, K. (1998). Calcium-induced exposure of a hydrophobic surface of mouse ALG-2, which is a member of the penta-EF-hand protein family. J. Biochem. *124*, 1170–1177.

Maki, M., Kitaura, Y., Satoh, H., Ohkouchi, S., and Shibata, H. (2002). Structures, functions and molecular evolution of the penta-EF-hand Ca^{2+}-binding proteins. Biochim. Biophys. Acta *1600*, 51–60.

Mella, M., Colotti, G., Zamparelli, C., Verzili, D., Ilari, A., and Chiancone, E. (2003). Information transfer in the penta-EF-hand protein sorcin does not operate via the canonical structural/functional pairing: a study with site-specific mutants. J. Biol. Chem. *278*, 24921–24928.

Missotten, M., Nichols, A., Rieger, K., and Sadoul, R. (1999). Alix, a novel mouse protein undergoing calcium-dependent interaction with the apoptosis-linked-gene 2 (ALG-2) protein. Cell Death Differ. *6*, 124–129.

Morita, E., and Sundquist, W.I. (2004). Retrovirus budding. Annu. Rev. Cell Dev. Biol. *20*, 395–425.

Morita, E., Sandrin, V., Chung, H.Y., Morham, S.G., Gygi, S.P., Rodesch, C.K., and Sundquist, W.I. (2007). Human ESCRT and ALIX proteins interact with proteins of the midbody and function in cytokinesis. EMBO J. *26*, 4215–4227.

Murshudov, G.N., Vagin, A.A., and Dodson, E.J. (1997). Refinement of macromolecular structures by the maximum-likelihood method. Acta Crystallogr. D Biol. Crystallogr. *53*, 240–255.

Odorizzi, G. (2006). The multiple personalities of Alix. J. Cell Sci. *119*, 3025–3032.

Otwinowski, Z., and Minor, W. (1997). Processing of X-ray diffraction data collected in oscillation mode. Methods Enzymol. *276*, 307–326.

Rao, R.V., Poksay, K.S., Castro-Obregon, S., Schilling, B., Row, R.H., del Rio, G., Gibson, B.W., Ellerby, H.M., and Bredesen, D.E. (2004). Molecular components of a cell death pathway activated by endoplasmic reticulum stress. J. Biol. Chem. *279*, 177–187.

Sadoul, R. (2006). Do Alix and ALG-2 really control endosomes for better or for worse? Biol. Cell *98*, 69–77.

Satoh, H., Shibata, H., Nakano, Y., Kitaura, Y., and Maki, M. (2002a). ALG-2 interacts with the amino-terminal domain of annexin XI in a Ca^{2+}-dependent manner. Biochem. Biophys. Res. Commun. *291*, 1166–1172.

Satoh, H., Nakano, Y., Shibata, H., and Maki, M. (2002b). The penta-EF-hand domain of ALG-2 interacts with amino-terminal domains of both annexin VII and annexin XI in a Ca^{2+}-dependent manner. Biochim. Biophys. Acta *1600*, 61–67.

Shibata, H., Yamada, K., Mizuno, T., Yorikawa, C., Takahashi, H., Satoh, H., Kitaura, Y., and Maki, M. (2004). The penta-EF-hand protein ALG-2 interacts with a region containing PxY repeats in Alix/AIP1, which is required for the subcellular punctate distribution of the amino-terminal truncation form of Alix/AIP1. J. Biochem. *135*, 117–128.

Shibata, H., Suzuki, H., Yoshida, H., and Maki, M. (2007). ALG-2 directly binds Sec31A and localizes at endoplasmic reticulum exit sites in a Ca^{2+}-dependent manner. Biochem. Biophys. Res. Commun. *16*, 756–763.

Shibata, H., Suzuki, H., Kakiuchi, T., Inuzuka, T., Yoshida, H., Mizuno, T., and Maki, M. (2008). Identification of alix-type and non-alix-type ALG-2-binding sites in human phospholipid scramblase 3: differential binding to an alternatively spliced isoform and amino acid-substituted mutants. J. Biol. Chem. *283*, 9623–9632.

Strobl, S., Fernandez-Catalan, C., Braun, M., Huber, R., Masumoto, H., Nakagawa, K., Irie, A., Sorimachi, H., Bourenkow, G., Bartunik, H., et al. (2000). The crystal structure of calcium-free human m-calpain suggests an electrostatic switch mechanism for activation by calcium. Proc. Natl. Acad. Sci. USA *97*, 588–592.

Subramanian, L., Crabb, J.W., Cox, J., Durussel, I., Walker, T.M., van Ginkel, P.R., Bhattacharya, S., Dellaria, J.M., Palczewski, K., and Polans, A.S. (2004). Ca^{2+} binding to EF hands 1 and 3 is essential for the interaction of apoptosis-linked gene-2 with Alix/AIP1 in ocular melanoma. Biochemistry *43*, 11175–11186.

Tarabykina, S., Moller, A.L., Durussel, I., Cox, J., and Berchtold, M.W. (2000). Two forms of the apoptosis-linked protein ALG-2 with different Ca^{2+} affinities and target recognition. J. Biol. Chem. *275*, 10514–10518.

Tarabykina, S., Mollerup, J., Winding, P., and Berchtold, M.W. (2004). ALG-2, a multifunctional calcium binding protein? Front. Biosci. *9*, 1817–1832.

Todd, B., Moore, D., Deivanayagam, C.C., Lin, G.D., Chattopadhyay, D., Maki, M., Wang, K.K., and Narayana, S.V. (2003). A structural model for the inhibition of calpain by calpastatin: crystal structures of the native domain VI of calpain and its complexes with calpastatin peptide and a small molecule inhibitor. J. Mol. Biol. *18*, 131–146.

Vernarecci, S., Colotti, G., Ornaghi, P., Schiebel, E., Chiancone, E., and Filetici, P. (2007). The yeast penta-EF protein Pef1p is involved in cation-dependent budding and cell polarization. Mol. Microbiol. *65*, 1122–1138.

Verzili, D., Zamparelli, C., Mattei, B., Noegel, A.A., and Chiancone, E. (2000). The sorcin-annexin VII calcium-dependent interaction requires the sorcin N-terminal domain. FEBS Lett. *71*, 197–200.

Vagin, A., and Teplyakov, A. (1997). MOLREP: an automated program for molecular replacement. J. Appl. Crystallogr. *30*, 1022–1025.

Vito, P., Lacanà, E., and D'Adamio, L. (1996). Interfering with apoptosis: Ca^{2+}-binding protein ALG-2 and Alzheimer's disease gene ALG-3. Science *271*, 521–525.

Vito, P., Pellegrini, L., Guiet, C., and D'Adamio, L. (1999). Cloning of AIP1, a novel protein that associates with the apoptosis-linked gene ALG-2 in a Ca^{2+}-dependent reaction. J. Biol. Chem. *274*, 1533–1540.

Williams, R.L., and Urbé, S. (2007). The emerging shape of the ESCRT machinery. Nat. Rev. Mol. Cell Biol. *8*, 355–368.

Wu, F., Zhang, M., and Gong, W. (2001). Crystallization and preliminary crystallographic studies of an apoptosis-linked calcium-binding protein ALG-2. Acta Crystallogr. D Biol. Crystallogr. *57*, 1162–1163.

Xie, X., Dwyer, M.D., Swenson, L., Parker, M.H., and Botfield, M.C. (2001). Crystal structure of calcium-free human sorcin: a member of the penta-EF-hand protein family. Protein Sci. *10*, 2419–2425.